Chapter 4

Plasmonic Modes in Au and AuAg Nanowires and Nanowire Dimers Studied by Electron Energy Loss Spectroscopy

Ina Schubert and Maria Eugenia Toimil-Molares

Additional information is available at the end of the chapter

http://dx.doi.org/10.5772/intechopen.79189

Abstract

In this chapter, we review our recent work on the investigation of surface plasmon modes in metallic nanowires and nanowire dimers by means of electron energy loss spectroscopy combined with scanning transmission electron microscopy (STEM-EELS). Due to the very high spatial resolution, STEM-EELS is a powerful technique to visualize multipole order surface plasmon modes in nanowires and study the dependency of their resonance energies on different parameters such as nanowire dimensions or nanowire porosity. In addition, we investigate surface plasmon hybridization in nanowires separated by gaps of less than 10 nm or connected by small metallic bridges. In such structures new modes arise, which depend strongly on gap or bridge sizes. Experimental results are supported by finite element simulations. The investigated nanowires and dimers are fabricated by electrodeposition in etched ion-track templates, combined with a selective dissolution processes. The synthesis techniques and their advantages for the fabrication of plasmonic nanostructures are also discussed.

Keywords: gold, nanowires, nanogaps, nanowire dimers, surface plasmons, plasmon hybridization, electron energy loss spectroscopy, scanning transmission electron microscopy, electrodeposition, ion-track technology, etched ion-track membranes

1. Introduction

Over the past 20 years surface plasmons in metallic nanoparticles have attracted great attention due to their potential for many applications in the fields of sensing [1], light guiding [2] and

energy conversion [3]. Surface plasmons are collective electronic oscillations that can be excited by an external electric field. At the surface plasmon resonance wavelength of the nanoparticle, the excitation of the electronic oscillation results in high electric near-fields. In the far-field the resonance frequency is strongly scattered and absorbed, but less transmitted. The resonance frequency of a given nanoparticle depends strongly on parameters such as, for example, the shape, dimension, and composition [4, 5]. Therefore, besides the continuous progress on the study of plasmonic properties, also the development of suitable methods to synthesize plasmonic nanostructures with very well-controlled characteristics is of great importance both for basic research as well as for technological applications.

1.1. Surface plasmons in nanowires

Surface plasmons in nanowires can be excited in two different directions [6]. Longitudinal surface plasmons are oscillations that occur in the direction of the long nanowire axis, whereas transversal modes oscillate in the direction of the nanowire diameter. This makes nanowires especially interesting for both plasmonic basic research as well as applications. In particular, longitudinal modes attract great attention since by varying the length of the nanowires, the resonance frequency can be tuned accurately within a wide range; for Au and Ag wires from the visible to infrared frequencies [7–10]. In this frequency range, the specific spectroscopic finger print of many molecules is located. This can be used for molecular sensing by surface enhanced infrared spectroscopy (SEIRA) [1]. When the molecules are located close to a Au or Ag nanowire, the high electric fields generated by surface plasmons can strongly increase the molecular absorption signals, thus enhancing the sensitivity of the method. For Au nanowires, enhancement factors up to a factor of 10^5 were reported [1].

Surface plasmons in nanowires have been investigated for different kind of metals, as well as for alloy and segmented wires [11]. Compared to other metals, Au nanowires offer the advantages of being chemically stable and nontoxic. This is important because, since infrared light is less energetic that other radiation types, also in vivo applications of surface plasmons in these structures such as, for example, photothermal therapy are envisaged [12].

Another advantage of Au nanowires is the possibility of exciting multipolar modes in addition to the dipolar one (in analogy to standing waves in a resonator). Whereas in spherical particles these modes usually overlap, the geometry of the nanowires results in a clear energetic separation for several multipole orders [8, 13, 14].

Single Au nanowires are thus very interesting objects to obtain fundamental knowledge on the basics of surface plasmons. However, not only single nanowires but also complex systems consisting of more than one wire separated by small gaps of few nanometers or small metallic connections are attracting great interest [15–18]. In these kinds of structures coupling of the surface plasmons of the individual structures is possible, which results in many new modes and further enhanced electromagnetic fields [15, 19].

1.2. Electron energy loss spectroscopy

Electron energy loss spectroscopy (EELS) is a powerful technique to visualize surface plasmon modes in nanostructures. It benefits from the very high spatial resolution of the transmission

electron microscope (TEM) that allows to analyze surface plasmons at specific positions of the nanostructure, for example, by the tip or in a gap [14, 20–22], together with the very broad energy range from ~0.3 eV to several eV. Different from other high spatial resolution techniques such as cathodoluminescence in the TEM [23] or scanning near-field optical microscopy (SNOM) [8], EELS not only allows investigating bright modes that couple efficiently to light, but also dark modes [20, 24].

Surface plasmon measurements with EELS are based on the interaction of the traveling electrons in the TEM with the electric field corresponding to the surface plasmons (excited by the electron itself) [25, 26]. The energy loss of the electrons is equivalent to the energy that is necessary to excite a given surface plasmon mode. For measuring this energy loss a magnetic prism in the TEM is used, deflecting electrons dependent on their energy loss [27]. Two different measurement modes exist:

For scanning transmission electron microscopy combined with electron energy loss spectroscopy (STEM-EELS), the electron beam is scanned along a defined path. At each position, a spectrum is created at the dispersive plane. The energy resolution of this technique is given by the natural energy width of the primary electrons that is decreased by a monochromator in the TEM to typically 0.1 eV. It is measured via the full width half maximum of the dominating zero loss peak of the spectrum. The high spatial resolution of the technique allows visualizing two dimensional EEL probability maps in the surrounding of the nanostructure.

For energy filtered transmission electron microscopy (EFTEM), a moveable slit is inserted at the position of the dispersive plane. Only electrons with a specific energy loss can pass the slit (typical slit width 0.2 eV) and deliver at the image plane a 2D image of the nanostructure. This image is created only by electrons with energy loss in the given range. In contrast to STEM-EELS, the energy resolution is worse but the measurement technique is faster.

For a more detailed introduction into the technique, the reader is referred to the following review articles [26, 28–30].

In this chapter, we review our recent activities on the investigation of surface plasmon modes in metallic nanowires and nanowire dimers by STEM-EELS. In Section 2, the synthesis of various Au-based nanowires by electrodeposition in etched ion-track membranes is presented, including Au and $Au_{1-x}Ag_x$ wires, as well as the fabrication of porous Au wires by subsequent dealloying of $Au_{0.4}Ag_{0.6}$ nanowires [31]. Following, the visualization of multipole order surface plasmon modes in these nanowires by STEM-EELS and the study of their resonance energies as a function of, for example, nanowire dimensions and nanowire porosity, is discussed [14, 32]. Section 3 describes the synthesis of nanowire dimers by electrodeposition of segmented Au-rich/Ag-rich/Au-rich nanowires and the subsequent dissolution of Ag [33]. It continues presenting STEM-EELS measurements on these nanostructures, which allowed the investigation of surface plasmon hybridization in nanowires separated by gaps of less than 10 nm [14] as well as connected by small metallic bridges [34]. In such structures, new modes arise that depend strongly on gap or bridge sizes, respectively. Section 3 finishes with discussing mode coupling of heterodimers consisting of two wires with different length [35]. All experimental results are supported by representative finite element calculations. The chapter concludes with a summary and final conclusions, both presented in Section 4.

2. Single nanowires

Recently, EELS analysis of metallic nanowires and rods consisting of Au [14, 20, 32, 36–38], Ag [13, 39, 40] and Al [41] demonstrated that it is an excellent technique to study their surface plasmon modes. Au nanorods with length up to 400 nm have been investigated by several authors using STEM-EELS and EFTEM visualizing their first- and second-order multipolar modes [20, 36–38]. In this chapter, we focus on our recent EELS investigations of the multipole order surface plasmon modes up to the seventh order in individual Au nanowires with 1–2 μm length and 60–100 nm diameter. The resonance energies were analyzed with respect to specific tailored wire parameters, such as length and diameter [14], composition and porosity [32] by STEM-EELS at Stuttgart Center for Electron Microscopy using a Zeiss SESAM transmission electron microscope operated at 200 keV. In this section, we first describe the fabrication of both smooth and porous Au nanowires by ion-track technology and electrodeposition and then summarize our results on the investigation of their plasmonic properties.

2.1. Synthesis of Au nanowires by ion-track technology and electrodeposition

The Au nanowires discussed in this chapter are fabricated by electrodeposition in etched ion-track membranes. The synthesis method is schematically displayed in **Figure 1** and involves the following separate processing steps: (1) irradiation of the template material (typically polymer foils with thickness 10–100 μm) with energetic heavy ions and creation of latent iontracks (**Figure 1a**); (2) selective ion-track dissolution and formation of channels by chemical etching (**Figure 1b**); (3) preparation of a conductive back-electrode (**Figure 1c**); (4) electrodeposition of Au in the nanochannels (**Figure 1d**) and (5) dissolution of the polymer membrane (**Figure 1e**).

Etched ion-track membranes are widely used as templates for nanowire growth since the late 1990s. Control over the irradiation and etching conditions enables the production of various

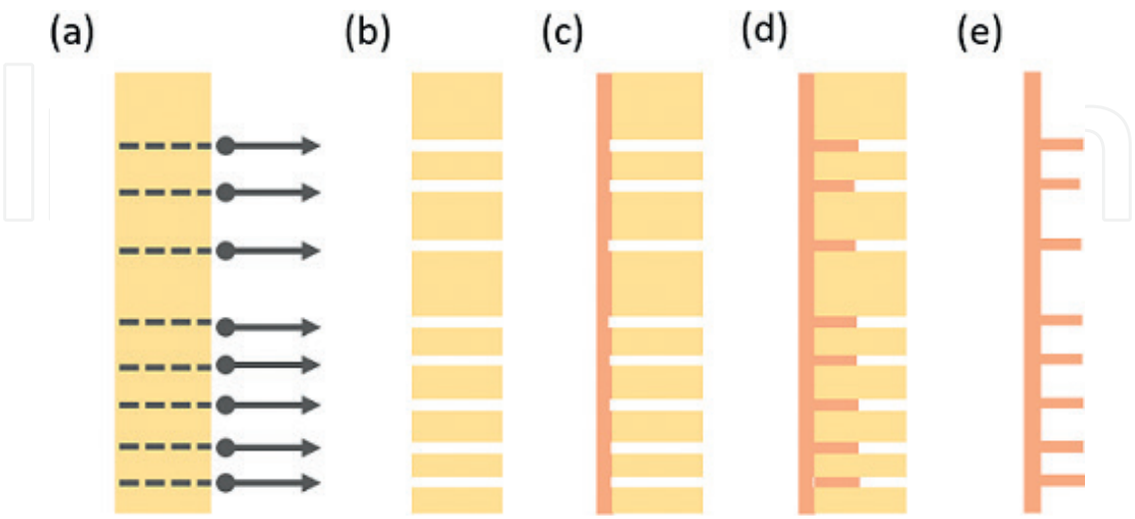

Figure 1. Schematics of the steps involved in the synthesis of Au-based nanostructures by the template method: (a) swift heavy ion irradiation of a polycarbonate foil and formation of ion-tracks (dotted lines), (b) selective chemical etching of the ion-tracks, (c) sputtering and electrochemical reinforcement of an electrical contact layer, (d) Au electrodeposition in the channels and (e) dissolution of the polymer foil.

http://dx.doi.org/10.5772/intechopen.79189

membranes with channels of predefined geometries (e.g., cylindrical, conical, bi-conical), with lengths varying between 1 and 100 μm, diameter ranging between ~15 nm up to several μm and aspect ratio (length *L* over diameter *D*) of up to 1000. Under suitable experimental conditions, the synthesized nanowires adopt the exact shape and size of the host channel, enabling thus the fabrication of wires with very well-controlled geometrical parameters. By varying the electrodeposition parameters, composition, crystallinity and crystallographic orientation of the deposited material can be adjusted. This unique combination of electrochemical deposition and etched ion-track membranes has demonstrated to be very powerful to synthesize nanowires with controlled and independently adjusted characteristics. In addition, a large number of wires up to 10^{10} cm^{-2} can be grown simultaneously.

Au nanowires with smooth contour were first electrodeposited using a two-electrode configuration, with the sputtered Au film as initial cathode and an Au rod as anode. Optimized growth conditions enabled the synthesis of both single- and polycrystalline cylindrical Au wires with diameters between 20 and 1000 nm [42–44] in a controlled manner. It was found that the employed electrolyte strongly influenced the crystalline structure of the deposited material. Thus, Au nanowires deposited with ammonium gold(I) sulfite (gold content = 15 g/L, Metakem GmbH, Usingen, Germany) or sodium disulfitoaurate (I) Imabrite 24 bath (gold content = 12.3 g/L, Schloetter Galvanotechnik, Geislingen/Steige, Germany) electrolytes exhibit a polycrystalline structure. In contrast, Au wires grown in a solution of potassium dicyanoaurate(I) (Puramet 402 bath, gold content = 10 g/L, Doduco, Pforzheim, Germany) yield single crystals at temperatures between 50 and 65°C under both direct-current and reverse-pulse deposition conditions. The resulting single-crystalline wires have a preferred [110] orientation independently of applied voltage and temperature.

Recently, this method has also been applied to prepare Au nanowires with smooth and rough contour, by electrodepositing Au in polycarbonate and polyethylene theraphthalate membranes, whose etched nanochannels exhibit smooth and rough contours, respectively. **Figure 2** shows the SEM images of two representative Au nanowire arrays deposited using a two electrode configuration in **Figure 2a** polycarbonate and in **Figure 2b** polyethylene terephthalate membranes using a sulfite-based electrolyte (Metakem, pH 7.5).

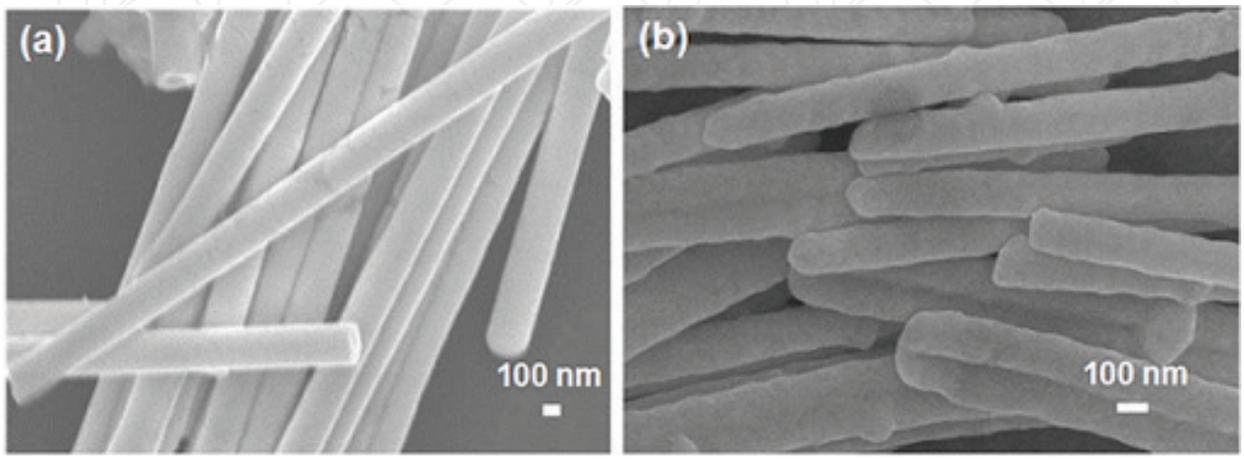

Figure 2. SEM image of Au nanowires deposited in (a) polycarbonate and (b) polyethylene terephthalate membranes. Reproduced with permission from [32]. Copyright VBRI press.

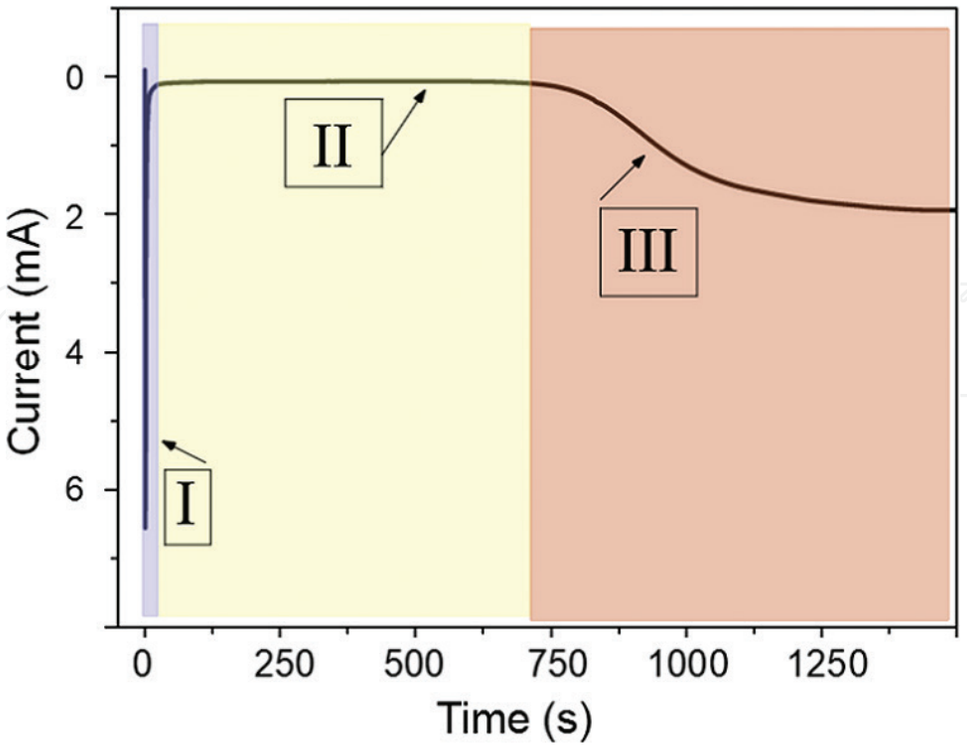

Figure 3. Current-versus-time curve recorded during the deposition of Au nanowires with a cyanide-based electrolyte. The three characteristic zones of nanowire growth are highlighted by the different colors.

For large-scale synthesis and industrial applications, two-electrode set-ups are most usual. However, it is known that the use of three electrodes improves the reproducibility and the control over the experiments. Therefore, subsequent synthesis of Au nanowires was investigated in a three-electrode configuration. The process was potentiostatic, using a Pt rod as counter electrode and a Ag/AgCl (Sat. KCl) reference electrode. In this case, a cyanide-based electrolyte consisting of $KAu(CN)_2$ (20 or 50 mM) and Na_2CO_3 (0.25 M) is employed. The voltage applied ranges between $U = -0.5$ and -1.1 vs. Ag/AgCl, and the temperature is kept constant at $T = 60°C$. The process is monitored by recording the current as a function of deposition time, that is, by chronoamperometry.

Figure 3 shows a representative current vs. time (*I-t*) curve recorded during the electrodeposition of Au nanowires from a cyanide solution. It reveals three different zones that are highlighted in the figure with different colors. In zone (I) at the moment of applying the potential, the absolute current increases and subsequently decreases (purple). This is due to the reduction of ions in the vicinity of the cathode and the formation of the diffusion layer, respectively. In zone (II), the current density remains almost constant (yellow). Due to their cylindrical geometry, the deposition area is constant during the growth of the material inside the channels. Once the nanochannels are filled, caps start to grow on top of the wires on the template surface. This enlarged surface area results in an increase of the absolute current value in zone (III) (red).

According to Faraday's law, the weight of a product of electrochemical reaction at an electrode is proportional to the electric charge *Q*, passing through the electrochemical cell. If the growth is homogeneous and the efficiency of the deposition reaction is 100%, the experimental charge, being the integral of the *I-t* curve, is thus equivalent to the theoretical value calculated applying Faraday's law:

http://dx.doi.org/10.5772/intechopen.79189

$$Q_{theo} = z\,F\,L \cdot \left(\frac{D}{2}\right)^2 \cdot \rho \cdot \frac{N_{\text{pores}}}{A_{\text{wt}}}, \quad (1)$$

where A_{wt} is the atomic weight of the deposit, z the number of electrons involved in the deposition, F Faraday's constant, D and L the nanowire diameter and length, ρ the density, and N_{pores} the number of pores in the membrane. For homogeneous nanowire growth, this enables to control the nanowire length. The deposition process is therefore stopped after the amount of charge necessary to obtain a specific wire length has been reached. In this way, Au nanowires with the same D and the same crystallography but different L, for example, between ~0.8 and ~30 μm can be synthesized.

2.2. Synthesis of porous Au nanowires

Compared to cylindrical smooth Au nanowires, porous Au wires exhibit larger surface areas and small nanovoids that can act as plasmonic hotspots, for example, for sensing [45, 46]. Porous Au wires can be also synthesized by the template method. Their fabrication was first demonstrated by Searson et al. [47, 48]. By using a single-bath electrolyte $Au_{1-x}Ag_x$ ($0 < x < 1$) alloy was deposited in the nanochannels. After dissolution of the template, the less noble material, in this case Ag, was selectively dissolved. Since then, various groups studied the influence of both initial AuAg wire composition and dealloying parameters on the resulting porosity, in most cases for wire diameters larger than 200 nm [49–52].

Recently, we reported the potentiostatic electrodeposition and characterization of thinner $Au_{1-x}Ag_x$ nanowires with controlled composition and size. The cylindrical $Au_{1-x}Ag_x$ nanowires exhibited three different D, namely, 85, 45 and 30 nm, and L between 10 and 20 μm and were analyzed with respect to their composition and morphology before and after dealloying.

Electrodeposition was performed at 60°C from aqueous electrolytes containing 0.25 M Na_2CO_3, as well as $KAu(CN)_2$ and $KAg(CN)_2$ in different ratios, namely (1) 50 mM of $KAu(CN)_2$ and 50 mM of $KAg(CN)_2$ (Au:Ag ratio 1:1) and (2) 50 mM of $KAu(CN)_2$ and 20 mM of $KAg(CN)_2$ (Au:Ag ratio 5:2). A constant potential of −1.1 V vs. Ag/AgCl reference electrode was applied and a platinum wire served as the counter electrode in all cases. After dissolution of the polymer foil, the wires were transferred onto silicon nitride TEM grids for posterior dealloying and analysis. For dealloying, the silicon nitride membranes with randomly distributed nanowires were immersed in 65% nitric acid (HNO_3, LS labor-Service GmbH) at room temperature for 3 h. The dealloying process of individual cylindrical wires with various sizes and compositions was characterized by means of TEM for the crystallinity and energy-dispersive X-ray spectroscopy (EDX) for the elemental analysis. The average composition measured by EDX-TEM for $Au_{1-x}Ag_x$ nanowires deposited using two different electrolyte compositions, before and after dealloying are reported in **Table 1**.

The EDX analysis of the as-grown nanowires before dealloying reveals two types of wires: Ag-rich nanowires (i.e., $Au_{0.4}Ag_{0.6}$) and Au-rich nanowires (i.e., $Au_{0.6}Ag_{0.4}$). The resulting wire compositions do not vary significantly as a function of channel diameter. **Figure 4** shows the corresponding dark-field TEM images of the nanowires. **Figure 4a, b** (left images) display the $Au_{0.4}Ag_{0.6}$ wires synthesized using an electrolyte with a ratio of $KAu(CN)_2$:$KAg(CN)_2$ = 1:1 with diameters of 85 nm (**Figure 4a**) and 45 nm (**Figure 4b**), respectively. **Figure 4c, d** (left images) display

$Au_{0.6}Ag_{0.4}$ wires with 85 and 45 nm diameter electrodeposited using a $KAu(CN)_2$:$KAg(CN)_2$ ratio of 5:2. Before dealloying, all nanowires are cylindrical and exhibit very smooth surfaces for all diameters and compositions. EDX with very high spatial resolution (below 1 nm) revealed the presence of a Ag-rich layer in $Au_{0.4}Ag_{0.6}$ wires and Au-rich layer in $Au_{0.6}Ag_{0.4}$ wires [31]. The thickness of these surface layers amounted 1–4 nm. After dealloying (right images), wires with very different morphologies are obtained. After dealloying in nitric acid, Ag-rich wires exhibit porous morphologies, whereas Au-rich wires remain solid cylinders displaying only a small increase in surface roughness. In **Figure 4e**, the EDX line scan shows the composition of a ligament of a dealloyed $Au_{0.4}Ag_{0.6}$ and evidences its almost pure Au composition across the ligament except for a small region (2–3 nm) with 20 at% of remaining Ag content. In turn, after dealloying,

	Before dealloying			After dealloying	
	Atomic % of Ag			Atomic % of Ag	
Initial wire diameter (nm)	85	45	30	85	45
Electrolyte:					
50 mM $KAu(CN)_2$	62 ± 4	60 ± 4	63 ± 3	8 ± 6	5 ± 6
50 mM $KAg(CN)_2$					
50 mM $KAu(CN)_2$	41 ± 4	38 ± 4	39 ± 3	39 ± 5	36 ± 3
20 mM $KAg(CN)_2$					

Reproduced with permission from Ref. [31]. Copyright 2015 American Chemical Society.

Table 1. Averaged Ag content (at%) in the nanowires measured by EDX spectroscopy before and after dealloying as a function of the initial wire diameter.

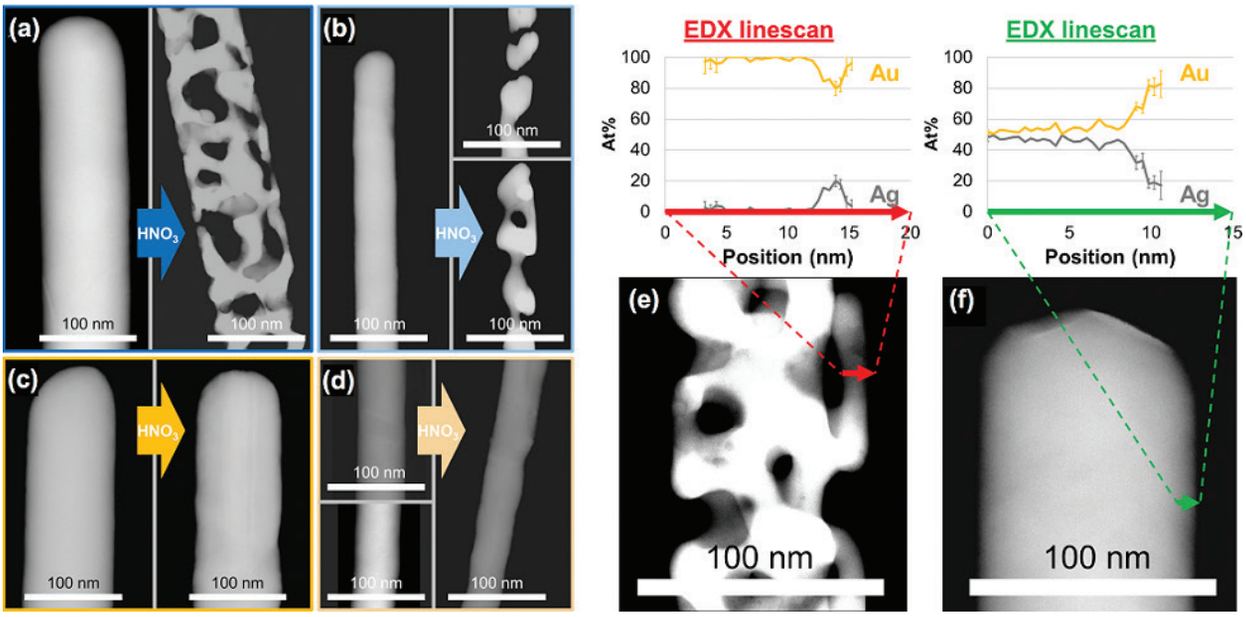

Figure 4. Dark-field TEM images of AuAg nanowires before (right) and after (left) dealloying in HNO_3: (a) $Au_{0.4}Ag_{0.6}$ nanowire, initial diameter 85 nm, (b) $Au_{0.4}Ag_{0.6}$ nanowire, initial diameter 45 nm, (c) $Au_{0.6}Ag_{0.4}$ nanowire, initial diameter 85 nm, (d) $Au_{0.6}Ag_{0.4}$ nanowire, initial diameter 45 nm. TEM image and EDX line scan across (e) a ligament of an $Au_{0.4}Ag_{0.6}$ dealloyed nanowire and (f) the surface of an $Au_{0.6}Ag_{0.4}$ nanowire after dealloying. Adapted with permission from [31] copyright 2015 American Chemical Society.

http://dx.doi.org/10.5772/intechopen.79189

the $Au_{0.6}Ag_{0.4}$ nanowires exhibit a diameter and composition similar to that of the initial nanowires (**Figure 4f**). They also have a relatively homogeneous Au-rich shell. This detailed analysis of the different Au-based nanowires, and in particular of their surface composition, is very important in order to interpret the plasmonic measurements presented in the following subsections, as well as for setting realistic inputs for simulations.

2.3. STEM-EELS of individual Au nanowires

Single cylindrical smooth Au nanowires with different aspect ratio were investigated by EELS to analyze their multipolar surface plasmon modes. **Figure 5** shows an example of a STEM-EELS map of a single Au nanowire with L = 895 nm ± 5 nm and D = 95 ± 5 nm. The map consists of 100 spectra that were recorded by scanning the electron beam along the red line on the right of the nanowire (distance to wire surface ~10 nm). Each horizontal line in the map corresponds to one single spectrum. The energy loss increases from left to right. The color in the map indicates the energy loss probability. The energy loss of an incident electron depends on the electromagnetic local density of states, projected in the direction of the traveling electron [25]. Thus, the energy loss maxima in the EELS map can be interpreted as the position of field maxima of standing surface plasmon waves. We can therefore identify different multipolar surface plasmon modes by counting these maxima. A single spectrum extracted from the map can be seen in **Figure 5b**, and the spectrum was recorded at the position of the red dot in the TEM image on the right.

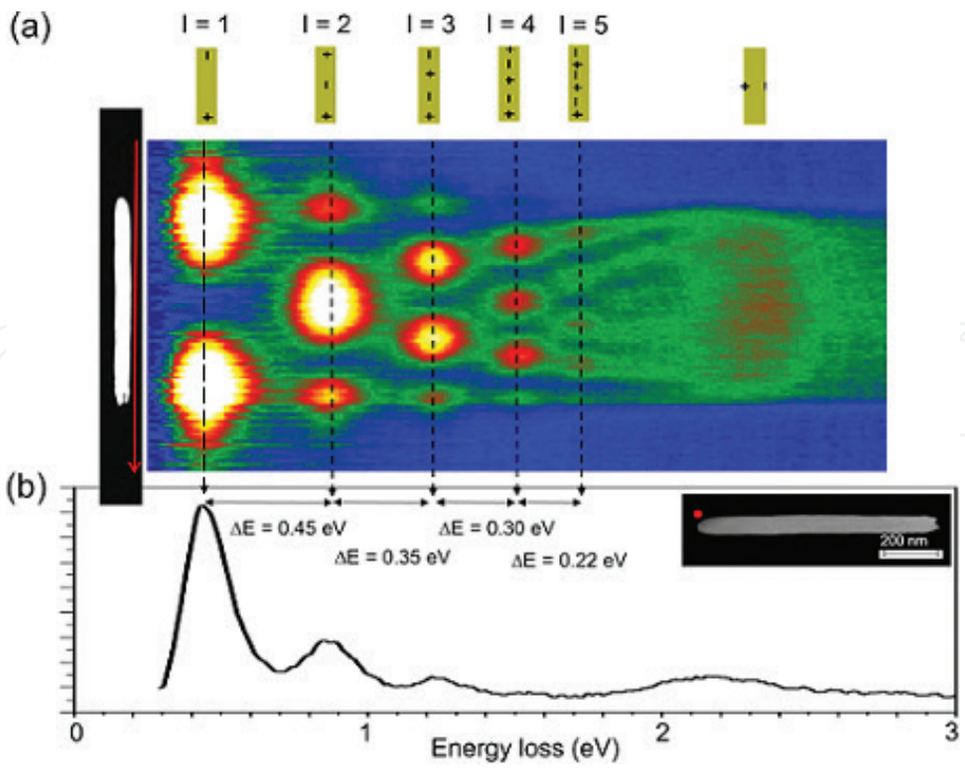

Figure 5. (a) STEM-EELS map of a single Au nanowire (L = 895 nm ± 5 nm; D = 95 ± 5 nm). The map consists of 100 spectra measured along the red arrow in the TEM image on the left. The schemes on top show the corresponding surface charge distributions; (b) single spectrum extracted from the map at the position of the red dot in the TEM image. Adapted with permission from [32]. Copyright VBRI press.

From the STEM-EELS map, it is possible to resolve surface plasmon modes of the wire in a broad energy interval between 0.4 and 2.7 eV. At low energies, the map clearly shows five different longitudinal modes of the Au nanowire as shown in the schemes on top of the map. At an energy of 2.3 eV, a transversal mode is excited all along the wire. To study the dependency of resonance energy versus nanowire dimensions, **Figure 6a** shows the energy of several multipole order longitudinal modes for 3 Au nanowires with different aspect ratios. It is seen that tuning the dimensions of the nanowire is a perfect tool to adjust the resonance energy of all multipole modes. TEM images of the three nanowires are depicted in **Figure 6b–d**. With increasing nanowire aspect ratio (L over D), the energies of all the longitudinal modes are shifted to lower energies, which is in accordance with results obtained with other measurement techniques and simulations (e.g., see [8–10]). The specific curve shape of the resonance energy versus multipole order for all three wires points toward a simple relation between these parameters. Using simulations, in 2007, Klebtsov et al. [6] have proposed the relation

$$\frac{1}{E} = A_0 + A_1 \cdot \frac{L/D}{l} \tag{2}$$

E is the energy of the respective mode and A_0 and A_1 are constants. Eq.(2) is motivated by the direct proportionality between L and the resonance wavelength λ of a perfect conductor, but is modified since penetration of light into the gold wire is possible in this frequency regime. **Figure 6e** shows a linear regression plot to the data of the three wires. Plotted is the inverse of the energy versus L/D over l according to Eq. 1. The relation follows well the data. As can be seen for the two wires with similar D (marked in black and green in **Figure 6e**), for wires of the same diameter and material of the same relation can be used to analytically calculate the multipole resonance energies.

2.4. STEM-EELS of porous nanowires

Another advantage of STEM-EELS is that wire details such as surface roughness or porosity can be resolved by the TEM together with the recording of the corresponding EELS map, enabling the investigation of how such specific parameters influence the resonance energies. **Figure 7** shows an example of a STEM-EELS map of a porous nanowire with $L = 1000 \pm 10$ nm

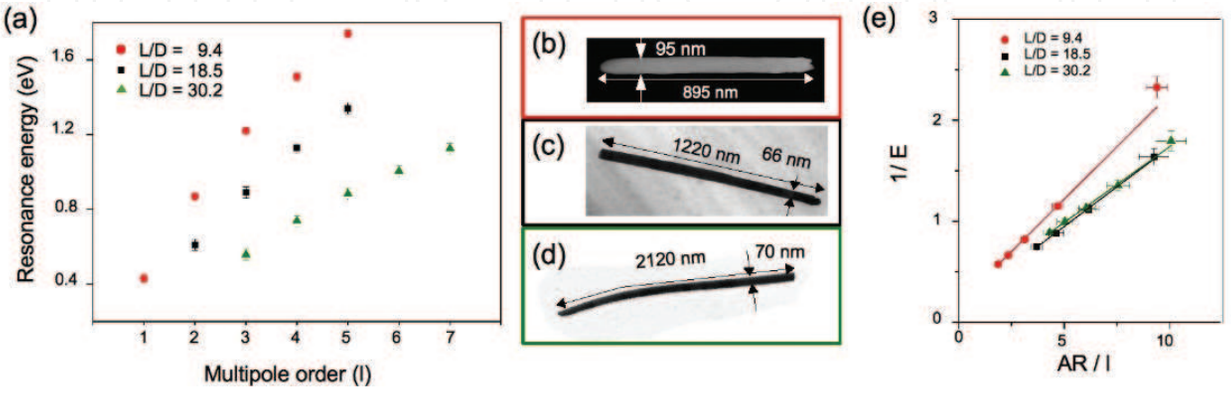

Figure 6. (a) Resonance energies for three different nanowires are plotted versus multipole order for the corresponding mode, (b) TEM images of the three different wires and (c) the inverse of the energy plotted versus aspect ratio over l for all three wires together with linear regression curves according to Eq. (2). Adapted with permission from [14]. Copyright 2011 American Chemical Society.

http://dx.doi.org/10.5772/intechopen.79189

and D = 90 ± 10 nm, thus with similar dimensions to the wire analyzed in **Figure 5**. For the longitudinal modes, the map resembles the one of the pure Au wire. However, at the higher energies (around approx. 2.2 eV, where we expect from the single Au wire the transversal mode), it is seen that the transversal mode of the porous wire is not excited at the same energy all along the nanowire, but the transversal mode energy shifts in a broad range between 1.9 and 2.3 eV dependent on the position. We account this to the varying pore sizes along the wire that can be seen in the TEM image in **Figure 7b**.

Since the porous wire is only slightly longer than the single Au wire in **Figure 5**, we can compare the energies of the respective modes. For all modes including the transversal, the energies measured for the porous wire are systematically lower than the corresponding mode energies of the continuous Au wire. This result is in agreement with further studies that we have conducted on the dipolar mode of Au nanowires by infrared spectroscopy [53] as well as results reported by other authors on shorter rods [54]. We believe that it can be explained by a change in the intrinsic parameters such as the lower bulk plasma frequency that follows from introducing an effective medium consisting of gold and empty voids to describe the porous material [53, 55].

2.5. Surface plasmon dispersion

EELS maps along individual nanowires allow deducing a surface plasmon dispersion relation. For this, the distance between two maxima, which corresponds to the half-surface plasmon wavelength of the respective mode, is measured [13, 40, 41]. Using this technique, different authors have derived dispersion relations for Ag [13, 40] and Al [41] nanowires by EFTEM

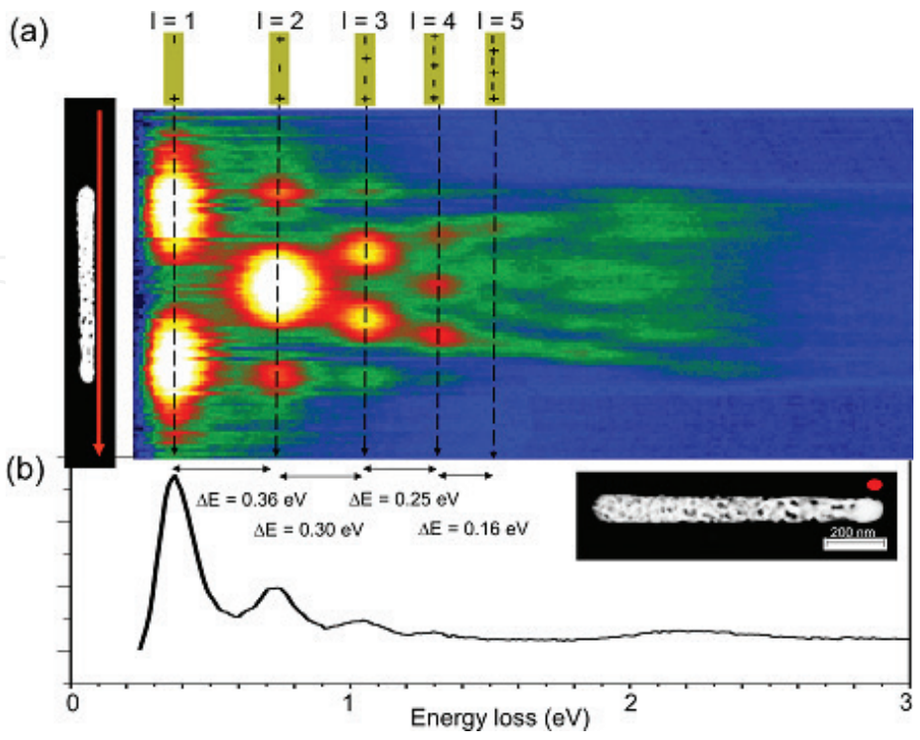

Figure 7. (a) STEM-EELS map consisting of 100 spectra measured along a porous Au nanowire (L = 1000 ± 10 nm, D = 90 ± 10 nm) together with the corresponding surface charge distributions; (b) single spectrum extracted from the map at the position of the red dot in TEM image. Adapted with permission from [32]. Copyright VBRI press.

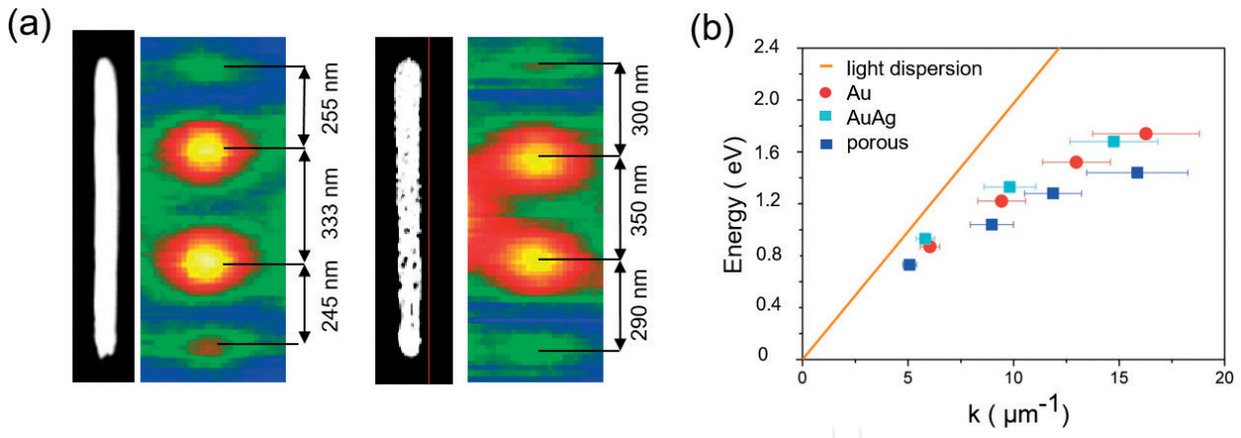

Figure 8. (a) Extract of the EELS map in **Figure 5** and **Figure 7** showing the surface plasmon half-wavelength of the third-order mode of smooth and porous nanowire and (b) dispersion relation for different Au-based nanowires together with the dispersion of light.

and STEM-EELS. For both materials, it was demonstrated that the distance between the maxima at the nanowire edges is shorter than the one between two maxima in the middle. The phenomenon is called antinode bunching [13] or λ_{sp} - compression [40]. It has been explained by a phase jump of the surface plasmon mode that is most probably due to the shape of the edges of the nanowire [13]. As it can be clearly seen exemplarily for the third-order mode of smooth and porous wires in **Figure 8a**, our data confirm this effect also for the Au wires. For both Ag and Al, it has been shown that the dispersion follows the shape of the calculated dispersion relation of fundamental surface plasmon polaritons sustained by an infinite Ag or respectively Al cylinder and that the low-order modes are close to the light line, which makes them easily excitable with light. **Figure 8b** shows the dispersion relation for a single Au nanowire, an $Au_{0.7}Ag_{0.3}$ alloy nanowire, and a porous Au wire. Values for the Au and AuAg alloy wire follow almost the identical curve shape, which we attribute to the similar dielectric function of Au and Ag at low energies and the small Ag content of only 30% in the wire. In contrast for the porous wire, the curve lies by trend below the one of the pure Au wire which we assign to a lower bulk plasma frequency as mentioned previously.

3. Coupled nanowire systems

Interaction between surface plasmons in several nanostructures that are separated by distances smaller than the decay length of the electric field is attracting a lot of attention in the field of plasmonics (see e.g., [15, 17, 19, 56–58]). In such systems, the plasmonic modes couple resulting in a splitting or hybridization (in analogy to molecular orbitals) in new plasmonic modes, called bonding and antibonding modes [16, 19, 56]. Nanowires are very interesting structures to study such hybridization phenomena, since their elongated shape results in a large energetic splitting of the modes even for higher multipole orders, which makes the splitting clearly resolvable in the energy loss spectrum. We have used systems consisting of two nanowires separated by small gaps [14, 35] or connected by small conductive bridges [34] to study such coupling effects. Taking up the terminology of molecular orbitals, the structures

are called 'nanowire dimers' [16]. After presenting our synthesis technique, we start the discussion with a dimer consisting of two wires with almost identical *L* and separated by a small gap, and continue with more complex structures such as wires connected by bridges or consisting of wires of different *L*.

3.1. Synthesis of nanowire dimers

The template method enables the synthesis of axially segmented nanowires composed by two or more materials. Back in the 1990s, the synthesis of segmented Cu/Co and Ni/Cu multilayer nanowires was reported [59, 60]. Since then, many different segmented structures combining, for example, polymers, semiconductors, and metals, have been fabricated by the template method [61, 62]. Segmented nanowires can be grown either by sequential exchange of the electrolyte [63, 64] or using a single-bath electrolyte and controlling the composition of the segments by tuning reduction potential and electrolyte composition [65, 66]. The combination of electrodeposition of segmented nanowires formed by two different materials, and the selective dissolution of the less noble, is known as on-wire lithography [67]. The Au nanowire dimers analyzed in this chapter are synthesized also in a similar two-step process. The first step consists of depositing segmented Au-rich/Ag-rich/Au-rich nanowires by sequential potentiostatic deposition, using the same electrolyte mentioned in Section 2.2, namely 0.25 M Na_2CO_3, and $KAu(CN)_2$ and $KAg(CN)_2$ in different concentrations [33]. The length of the Ag and Au segments is controlled by the duration of the corresponding pulses. Each segment contains a certain amount of the second metal. However, potential and electrolyte concentration can be chosen such that the relative concentration of the second material remains low (< 40%). After dissolution of the polycarbonate template using dichloromethane, the nanowires are transferred on to silicon nitride membranes. By immersing the substrate into concentrated nitric acid for 3 h, the middle silver segment is selectively etched. The gap size is determined by the length of the Ag segment. Using this method, we reported the fabrication of nanogaps with sizes between 7 and 30 nm [33].

Figure 9 shows SEM images of two wires with *D* ~65 nm consisting of 6 Au-rich and 6 Ag-rich segments (a) before and (b) after the nitric acid treatment. It can be seen in **Figure 9b** that in some cases a small metallic connection remains between the Au-rich segments. In this case, adjacent nanowire segments are electrically connected by the small junction. The small connections can be efficiently removed by thermal annealing at 300°C for 30 min, resulting in adjacent Au segments of similar length separated by a well-defined gap, as shown exemplary in **Figure 9c**.

This method has been applied to produce adjacent nanowires of controlled length separated by a gap of predesigned properties. Thus, two adjacent nanowires with similar length separated by a narrow gap are referred to as "nanowire dimers." If different pulse durations are applied for the first and third pulses, dimers consisting of Au segments with different length are produced. These are referred to as "nanowire heterodimers" or "symmetry broken dimers." In addition, two nanowires joined by a small metallic remaining connection (**Figure 9b**) are conductively coupled, while the two wires separated by a well-defined gap (**Figure 9c**) are capacitively coupled. In the next sections, we discuss the plasmonic properties of different nanowire dimers and heterodimers produced by this method.

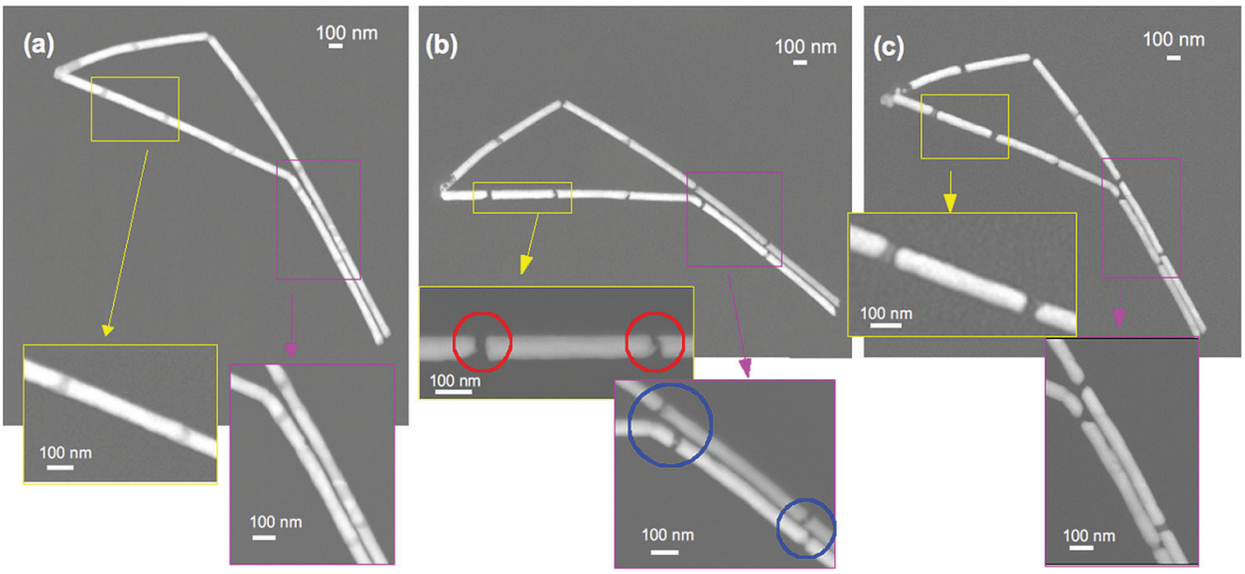

Figure 9. (a) SEM image of two segmented nanowires obtained applying a six pulse sequences consisting each of U_1 = −1.1 V (25 s) and U_2 = −0.5 V (15 s) vs. Ag/AgCl. (b) the same two nanowires after treatment with nitric acid. Small metal junctions are seen between some of the nanowires. (c) Nanowires after nitric acid treatment and annealing at 300°C for 30 min. Well-defined gaps are formed. Adapted from [33], an article distributed under public license https://www.beilstein-journals.org/bjnano/copyright; copyright the authors of [33].

3.2. Finite element simulation of coupled systems

Experimental results can be predicted, verified, or complemented by theoretical calculations of surface plasmons. For nanogaps larger than 1 nm quantum phenomena can usually be excluded [58]. In this case, classical calculations based on solving Maxwell's equation are conducted. Several different numerical methods are usually applied to study surface plasmon modes, such as the discrete dipole approximation [68], the boundary-element method [10, 15], or, as in our case, finite element simulations [69]. To conduct finite element simulations, commercial programs such as, for example, Comsol, Lumerical and CST Microwave Studio allow defining the plasmonic nanostructures with high accuracy. In the finite element codes, the structures are subdivided into a large amount of small volume elements. The electric field is numerically calculated by solving Maxwell's equations for these elements using suitable boundary conditions.

To analyze the surface plasmons in nanowires and coupled systems, we have performed finite element simulations with CST Microwave Studio [34]. To simulate the excitation of surface plasmons by a small point source, as it is the case during EELS measurements, we selected as excitation source a small dipole of impedance 5 kΩ located at 1 nm from the surface of the simulated Au nanostructure. This point source excites both bright and dark modes, and can be placed at different positions to analyze plasmon excitation as a function of the relative distance to the wire. **Figure 10** shows the finite element simulations of the electric field strength versus energy for four different structures: a nanowire dimer with gap of 19 nm (red line), two dimers with connections (green line: bridge length 19 nm and bridge diameter 20 nm; blue line: bridge length 19 nm and bridge diameter 40 nm) and a continuous wire. All nanostructures have a total L = 1145 nm including gap or connection and D = 90 nm. The spectra are normalized to the electric field of the dipole at the specific position for the situation that no Au nanostructure is present. In this simulation, the dipole is located 1 nm from one end of the nanostructures. All spectra are calculated 1 nm from the opposite end of the structures.

http://dx.doi.org/10.5772/intechopen.79189

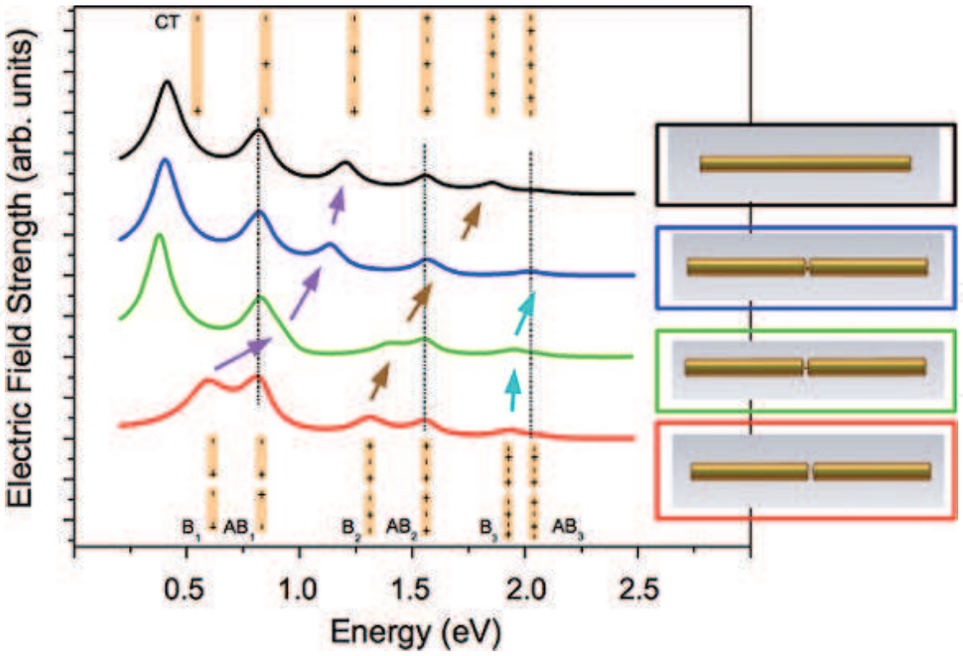

Figure 10. Finite element simulation of the electric field strength 1 nm from the end of a nanowire with gap (red), a dimer with small connection of diameter 20 nm (green), with larger connection of diameter 40 nm (blue) and a continuous wire (black). Reprinted with permission from [34]. Copyright 2012 American Chemical Society.

The figure also shows the corresponding charge distributions of the various modes that were obtained from the simulation. In the following sections, we refer to this figure when analyzing the STEM-EELS maps of the corresponding structures.

3.3. STEM-EELS of nanowire dimers with gaps

Figure 11a shows a STEM-EELS map of nanowire dimer consisting of two wires separated by a gap of about 8 nm. The two wires have length $L_1 = 784 \pm 5$ nm, $L_2 = 808 \pm 5$ nm, and a diameter of $D = 112 \pm 5$ nm. The map of the dimer differs from the ones of single wires by the energy separation between consecutive modes. For a single wire, the energy difference between two consecutive modes decreases with energy (see **Figure 5**). In contrast, for this dimer we find three pairs of modes that are closer in energy than the difference to the next pair. The black arrows below the map depict the energy difference between two modes corresponding two a pair. Each pair consists of a bonding and an antibonding mode that are generated from the coupling of the modes of the two individual wires. The bonding mode is the one having two surface charge maxima of different polarity at the two gap sides, whereas the antibonding mode possesses two maxima of same polarity at this position. In **Figure 11c**, the hybridization scheme of the dimer is schematically shown for the first three multipole orders. These mode pairs of bonding and antibonding modes can also be clearly seen in the red spectrum of **Figure 10** showing the simulation of a nanowire dimer.

The missing energy loss maxima of the bonding modes at the position of the gap can be understood from symmetry reasons. When placing the electron beam at the position of the gap no asymmetric charge distribution can be excited. In addition to the longitudinal modes, the map reveals also a transversal mode of the dimer that can be excited all along the two wires but not at the position of the gap. In the case of dimers, both aspect ratio of the wires and gap

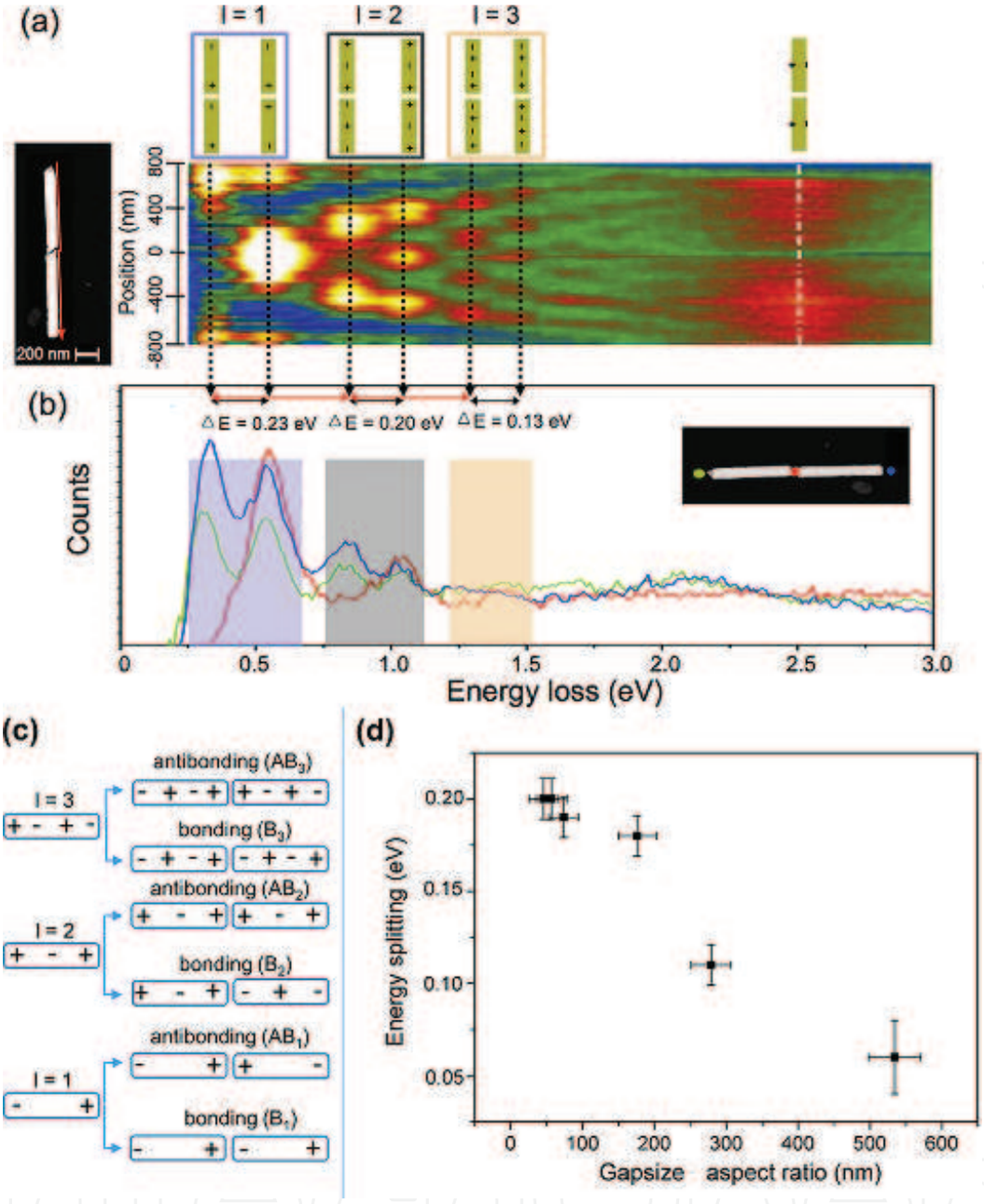

Figure 11. (a) STEM-EELS map of nanowire dimer with a gap of about 8 nm. On top of the map the corresponding surface charge distributions of the modes are shown, (b) three spectra measured at the position of the colored dots in the TEM image, (c) hybridization scheme of the dimer for the first three multipole orders and (d) energy splitting for the $l = 2$ bonding and antibonding modes versus gap size times aspect ratio. Adapted with permission from [14] copyright 2011 American Chemical Society.

size influence the energy splitting of the bonding and antibonding modes. For the $l = 2$ modes, the energy difference between bonding and antibonding mode is plotted in **Figure 11d** versus aspect ratio times gap size.

3.4. STEM-EELS of coupled nanowires connected by small bridges

Calculations reported in several publications predict that conductively coupled metallic objects can result in extremely conductance sensitive shifts of the resonance energies [18, 57, 70–74].

http://dx.doi.org/10.5772/intechopen.79189

Such structures are therefore promising platforms for sensing and optical switching applications [18, 74]. Due to difficulties in preparing such structures with controlled dimensions, experimental studies are still rare [21]. As explained in Section 3.1, during the synthesis of nanowire dimers by on-wire lithography from segmented AuAg nanowires, small conductive junctions can remain between two adjacent wires (e.g., **Figure 9b**). This allowed us to perform STEM-EELS analysis on such nanowire dimers with small connections attaining reliable data on the plasmonic properties of these promising systems [34].

Figure 12 shows a STEM-EELS map of a nanowire dimer where the gap is not completely dissolved, so that a conductive gold bridge remains between the two nanowires. For the dimer, L = 1145 ± 10 nm and D = 90 ± 10 nm. Clearly, seven different multipolar modes can be distinguished that reveal a complex arrangement in energy that differs from the one of a capacitively coupled dimer and as well from the one of a single wire. The schematics on top of the map reveal the charge distribution of these modes that have been identified by simulations of such connected structures (**Figure 10**).

In **Figure 10**, one can see that modes with symmetrical charge distribution (the antibonding modes of the nanowire dimer) do not shift in energy independent on connection size or if a gap is present, whereas all modes of unsymmetrical charge distribution (the bonding modes

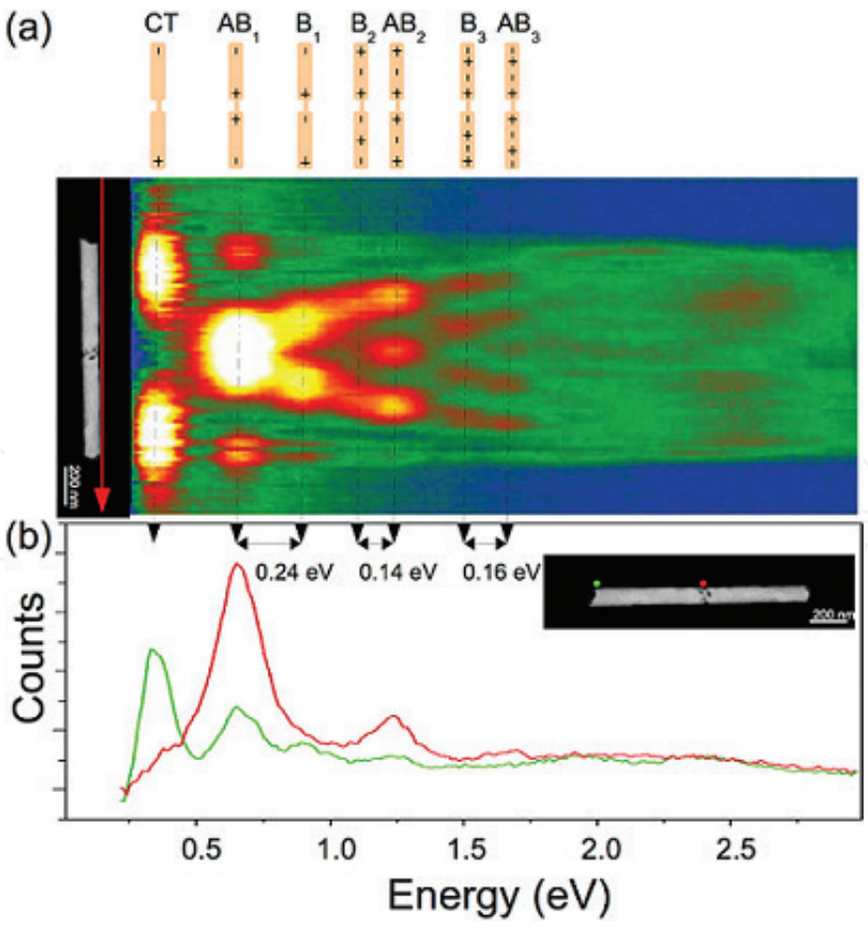

Figure 12. (a) STEM-EELS map of a nanowire dimer with metallic connection. (b) Two spectra extracted at the positions of the colored dots in the TEM image. Reprinted with permission from [34]. Copyright 2012 American Chemical Society.

of the nanowire dimer) shift continuously to higher energies with increasing connection size. The strength of the shift decreases with increasing multipole order and results thus in the arrangement seen in **Figure 12** where the bonding mode of first order (labeled with B_1 in the figure) is located at higher energy than the corresponding antibonding mode (AB_1). However, bonding modes of second and third order (B_2 and B_3) are observed at lower energies than the corresponding antibonding modes (AB_2 and AB_3).

The shift of the bonding modes is related to the electric field distribution of the wire in the gap. Therefore, the field distribution of a connected dimer and a continuous wire for modes with formally same number of surface charge maxima should be compared. **Figure 13** shows the electric field distributions of the second-order antibonding mode of the connected dimer (**Figure 13a**) and the l = 4-mode of the continuous wire (**Figure 13b**). Since for antibonding modes the space in the gap is almost field-free, these two modes have identical field distributions and are excited at the same energy. For the field distributions of the second-order bonding mode of the dimer (**Figure 13c**) and the l = 5-mode or the continuous wire (**Figure 13d**) the situation is different: Here a strong field is excited in the gap, shifting the charge maxima in the direction of the gap. The shift to higher energies of the bonding modes is linked to this electric field strength in the gap and decreases thus with increasing multipole order resulting in a completely new mode arrangement compared to dimers with gap.

3.5. Mode coupling in heterodimers

Up to now, we have focused only on surface plasmon coupling in structures consisting of two wires with very similar dimensions. In literature, several examples of mode coupling in nanostructures of different material [74–78] or dimensions [35, 79–82] have been reported. **Figure 14** shows clear evidence that surface plasmon coupling is also possible in heterodimers even between modes of different multipole order. The dimer has a diameter D = 76 nm ± 5 nm and consists of two wires with length L_1 = 656 nm ± 10 nm and L_2 = 1036 nm ± 10 nm; the gap size is ~12 nm. **Figure 14a** presents a STEM-EELS map of the dimer. In this map, nine different modes can be identified that are labeled with Arabic numbers on top of the map. In addition, **Figure 14b** shows an EFTEM series of the same dimer. A step size between the images of 0.2 eV (which corresponds also to the slit width) was used. Each image of the series is plotted next to the corresponding mode in the STEM-EELS map. It can be seen that for

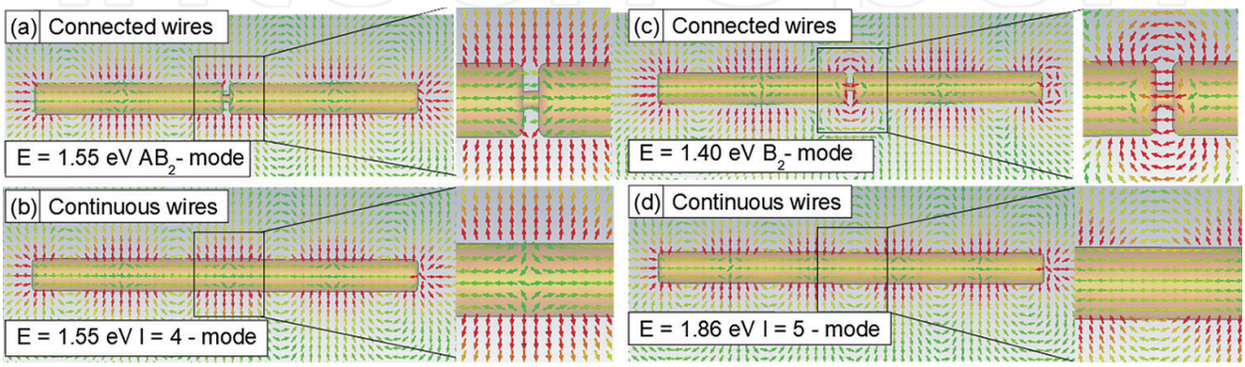

Figure 13. Calculated field distributions for the second-order (a) antibonding and (b) bonding mode of the connected dimer and the (c) l = 4 and (d) l = 5 mode of the continuous wire. Reprinted with permission from [34]. Copyright 2012 American Chemical Society.

http://dx.doi.org/10.5772/intechopen.79189

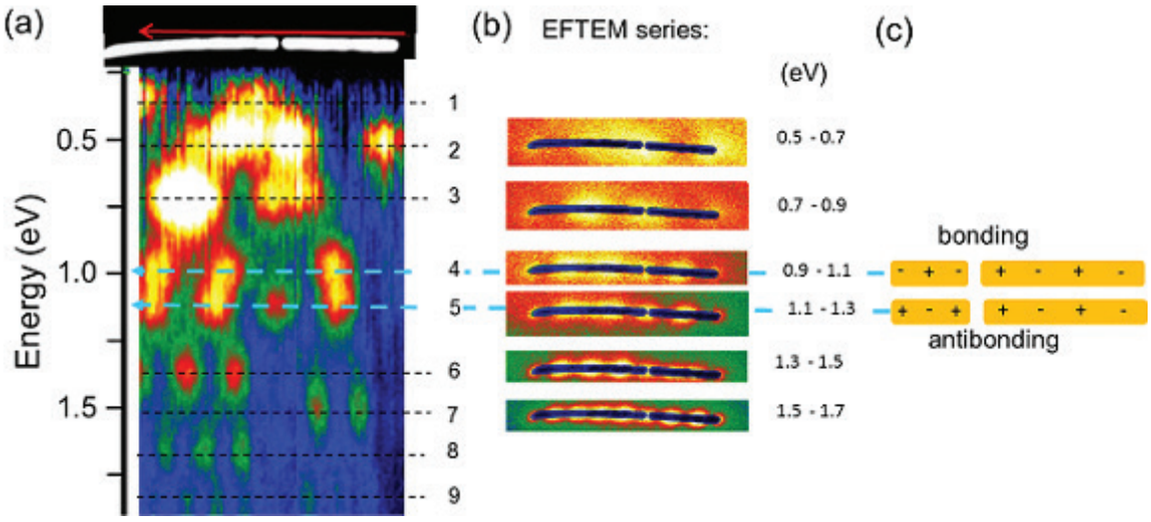

Figure 14. (a) EFTEM series of a nanowire heterodimer with 12 nm gap, (b) STEM-EELS map of the same dimer; (c) scheme of the bonding and antibonding mode pair. Adapted from [35] with permission from the Royal Society of Chemistry.

most of the modes, the plasmon mode is more intense either in the long or in the short wire. However, for the modes labeled with 4 and 5, the maxima are very intense along both wires: in this energy interval, in the short wire, the second-order mode ($l_1 = 2$) is active, whereas in the longer wire the third-order mode ($l_2 = 3$) is excited. Both modes couple and form a pair of bonding and antibonding modes as shown schematically in **Figure 14c**. An evidence of such a pair is visible in particular in the STEM map since no maxima can be seen at the gap for mode number 4 which is a typical feature of the bonding mode. The required condition for mode splitting in such unsymmetrical dimers is that in both of the individual wires a mode is excited at almost the same energy as another mode in the second wire, that is, spectral overlap between the two modes of the individual wires has to occur. As follows from Eq. (2), for nanowires, this can, for example, be achieved by designing dimers with length ratio $L_2/L_1 = l_2/l_1$, where l_2 and l_1 are the multipole orders of the two corresponding modes of the individual wires. In the shown dimer, $L_2/L_1 = 1.58 \pm 0.03$, is deviating only slightly from the ratio between the corresponding multipole orders $l_2/l_1 = 3/2$. Simulations also confirm the spectral overlap of these two modes (see [35]).

4. Conclusions

We have shown that STEM-EELS is an extremely powerful technique to analyze surface plasmon modes in nanostructures, and in particular, in nanowires and nanowire dimers. Thanks to its very high spatial resolution, it has been possible to investigate resonance energies of multipole order surface plasmon modes, measure surface plasmon dispersion relations, as well as to analyze surface plasmon excitation on specific positions along the nanostructures.

Cylindrical nanowires are synthesized by electrodeposition in etched ion-track membranes, combined with dealloying. This combination enables the fabrication of nanowires with excellent control on dimension (length, diameter), porosity and composition. These wires are, therefore, excellent model systems to analyze the influence of each parameter on the surface

plasmons. Thus, EELS data evidence lower resonance energies for porous wires compared to smooth ones of similar dimensions for both longitudinal and transversal modes. Also, the dispersion relation for the porous nanowires is slightly different from the one of Au and $Au_{0.7}Ag_{0.3}$ nanowires, most probably due a lower bulk plasma frequency of the porous material.

Symmetric and asymmetric dimers separated by small gaps, that is, capacitively coupled, are fabricated by the selective dissolution of short Ag segments in electrodeposited Au/Ag/Au segmented nanowires. In these structures, energy splitting in bonding and antibonding modes was experimentally visualized clearly up to the third multipolar order. If a small metallic junction remains between two adjacent wires, the wires are conductively coupled, and a completely new mode arrangement arises due to an energy shift of the bonding modes. The modes are strongly dependent on the connection size. Finally, mode coupling was also demonstrated for heterodimers consisting of two wires with different length. In these structures, mode coupling is possible if two modes of the individual wires do spectrally overlap. All experimental results are in excellent agreement with finite element calculations.

Acknowledgements

We acknowledge W. Sigle and P.A. van Aken from MPI Stuttgart for Solid State Physics for their help with EELS measurements and TEM-EDX of our nanowires. The authors thank C. Trautmann for fruitful discussion and her continuous support during the project, as well as L. Burr for his contribution in the synthesis and characterization of Au-based nanowires.

Author details

Ina Schubert* and Maria Eugenia Toimil-Molares

*Address all correspondence to: i.schubert@gsi.de

GSI Helmholtz Center for Heavy Ion Research GmbH, Darmstadt, Germany

References

[1] Neubrech F, Pucci A, Cornelius TW, Karim S, Garcia-Etxarri A, Aizpurua J. Resonant plasmonic and vibrational coupling in a tailored nanoantenna for infrared detection. Physical Review Letters. 2008;**101**:157403. DOI: 10.1103/PhysRevLett.101.157403

[2] Maier SA, Kik PG, Atwater HA, Meltzer S, Harel E, Koel BE, Requicha AAG. Local detection of electromagnetic energy transport below the diffraction limit in metal nanoparticle plasmon waveguides. Nature Materials. 2003;**2**:229-232. DOI: 10.1038/nmat852

[3] Clavero C. Plasmon-induced hot-electron generation at nanoparticle/metal-oxide interfaces for photovoltaic and photocatalytic devices. Nature Photonics. 2014;**8**:95-103. DOI:10.1038/nphoton.2013.238

[4] Link S, Mohamed MB, El-Sayed MA. Simulation of the optical absorption spectra of gold nanorods as a function of their aspect ratio and the effect of the medium dielectric constant. The Journal of Physical Chemistry. B. 1999;**103**:3073-3077. DOI: 10.1021/jp990183f

[5] Link S, Wang ZL, El-Sayed MA. Alloy formation of gold−silver nanoparticles and the dependence of the plasmon absorption on their composition. The Journal of Physical Chemistry. B. 1999;**103**:3529-3533. DOI: 10.1021/jp990387w

[6] Khlebtsov BN, Khlebtsov NG. Multipole plasmons in metal nanorods: Scaling properties and dependence on particle size, shape, orientation, and dielectric environment. Journal of Physical Chemistry C. 2007;**111**:11516-11527. DOI: 10.1021/jp072707e

[7] Schider G, Krenn JR, Hohenau A, Ditlbacher H, Leitner A, Aussenegg FR, Schaich WL, Puscasu I, Monacelli B, Boreman G. Plasmon dispersion relation of Au and Ag nanowires. Physical Review B. 2003;**68**:155427. DOI: 10.1103/PhysRevB.68.155427

[8] Dorfmüller J, Vogelgesang R, Weitz RT, Rockstuhl C, Etrich C, Pertsch T, Lederer F, Kern K. Fabry-Pérot resonances in one-dimensional plasmonic nanostructures. Nano Letters. 2009;**9**:2372-2377. DOI: 10.1021/nl900900r

[9] Neubrech F, Kolb T, Lovrincic R, Fahsold G, Pucci A, Aizpurua J, Cornelius TW, Toimil-Molares ME, Neumann R, Karim S. Resonances of individual metal nanowires in the infrared. Applied Physics Letters. 2006;**89**:253104. DOI: 10.1063/1.2405873

[10] Bryant G, Garcia de Abajo FJ, Aizpurua J. Mapping the Plasmon resonances of metallic Nanoantennas. Nano Letters. 2008;**8**:631-636. DOI: 10.1021/nl073042v

[11] Cortie MB, McDonagh AM. Synthesis and optical properties of hybrid and alloy plasmonic nanoparticles. Chemical Reviews. 2011;**111**:3713-3735. DOI: 10.1021/cr1002529

[12] Alkilany AM, Thompson LB, Boulos SP, Sisco PN, Murphy CJ. Gold nanorods: Their potential for photothermal therapeutics and drug delivery, tempered by the complexity of their biological interactions. Advanced Drug Delivery Reviews. 2012;**64**:190-199. DOI: 10.1016/j.addr.2011.03.005

[13] Rossouw D, Couillard M, Vickery J, Kumacheva E, Botton GA. Multipolar plasmonic resonances in silver nanowire antennas imaged with a subnanometer electron probe. Nano Letters. 2011;**11**:1499-1504. DOI: 10.1021/nl200634w

[14] Alber I, Sigle W, Müller S, Neumann R, Picht O, Rauber M, van Aken PA, Toimil-Molares ME. Visualization of multipolar longitudinal and transversal surface plasmon modes in nanowire dimers. ACS Nano. 2011;**5**:9845-9853. DOI: 10.1021/nn2035044

[15] Aizpurua J, Bryant GW, Richter LJ, Garcia de Abajo FJ. Optical properties of coupled metallic nanorods for field-enhanced spectroscopy. Physical Review B. 2005;**71**:235420. DOI: 10.1103/PhysRevB.71.235420

[16] Willingham B, Brandl DW, Nordlander P. Plasmon hybridization in nanorod dimers. Applied Physics B: Lasers and Optics. 2008;**93**:209-216. DOI: 10.1007/s00340-008-3157-5

[17] Qin L, Zou S, Xue C, Atkinson A, Schatz GC, Mirkin CA. Designing, fabricating, and imaging Raman hot spots. PNAS. 2006;**103**:13300-13303. DOI: 10.1073/pnas.0605889103

[18] Perez-Gonzalez O, Zabala O, Borisov AG, Halas NJ, Nordlander P, Aizpurua J. Optical spectroscopy of conductive junctions in plasmonic cavities. Nano Letters. 2010;**10**:3090-3095. DOI: 10.1021/nl1017173

[19] Nordlander P, Oubre C, Prodan E, Li K, Stockman MI. Plasmon hybridization in nanoparticle dimers. Nano Letters. 2004;**4**:899-903. DOI: 10.1021/nl049681c

[20] Chu MW, Myroshnychenko V, Chen CH, Deng JP, Mou CY, Garcia de Abajo FJ. Probing bright and dark surface-plasmon modes in individual and coupled noble metal nanoparticles using an electron beam. Nano Letters. 2009;**9**:399-404. DOI: 10.1021/nl803270x

[21] Duan H, Fernandez-Dominguez AI, Bosman M, Maier SA, Yang JKW. Nanoplasmonics: Classical down to the nanometer scale. Nano Letters. 2012;**12**:1683-1689. DOI: 10.1021/nl3001309

[22] Nelayah J, Kociak M, Stéphan O, Garcia de Abajo FJ, Tencé M, Henrard L, Taverna D, Pastoriza-Santos I, Liz-Marzán LM, Colliex C. Mapping surface plasmons on a single metallic nanoparticle. Nature Physics. 2007;**3**:348-353. DOI: 10.1038/nphys575

[23] Myroshnychenko V, Nelayah J, Adamo G, Geuquet N, Rodríguez-Fernández J, Pastoriza-Santos I, MacDonald KF, Henrard L, Liz-Marzán LM, Zheludev NI, Kociak M, García de Abajo FJ. Plasmon spectroscopy and imaging of individual gold nanodecahedra: A combined optical microscopy, cathodoluminescence, and electron energy-loss spectroscopy study. Nano Letters. 2012;**12**:4172-4180. DOI: 10.1021/nl301742h

[24] Koh AL, Bao K, Khan I, Smith WE, Kothleitner G, Nordlander P, Maier SA, McComb DW. Electron energy-loss spectroscopy (EELS) of surface plasmons in single silver nanoparticles and dimers: Influence of beam damage and mapping of dark modes. ACS Nano. 2009;**3**:3015-3022. DOI: 10.1021/nn900922z

[25] Garcıa de Abajo FJ, Kociak M. Probing the photonic local density of states with electron energy loss spectroscopy. Physical Review Letters. 2008;**100**:106804. DOI: 10.1103/PhysRevLett.100.106804

[26] Garcia de Abajo FJ. Optical excitations in electron microscopy. Reviews of Modern Physics. 2010;**82**:210-262. DOI: 10.1103/RevModPhys.82.209

[27] Sigle W. Analytical transmission electron microscope. Annual Review of Materials Research. 2005;**35**:239-314. DOI: 10.1146/annurev.matsci.35.102303.091623

[28] Kociak M, Stéphan O, Gloter A, Zagonel LF, Tizei LH, Tencé M, March K, Blazit JD, Mahfoud Z, Losquin A, Meuret S, Colliex C. Seeing and measuring in colours: Electron microscopy and spectroscopies applied to nano-optics. Comptes Rendus Physique. 2014;**15**:158-175. DOI: 10.1016/j.crhy.2013.10.003

[29] Kociak M, Stéphan O. Mapping plasmons at the nanoscale in an electron microscope. Chemical Society Reviews. 2014;**43**:3865. DOI: 10.1039/C3CS60478K

[30] Colliex C, Kociak M, Stéphan O. Electron energy loss spectroscopy imaging of surface plasmons at the nanometer scale. Ultramicroscopy. 2016;**162**:A1-A24. DOI: 10.1016/j.ultramic.2015.11.012

[31] Burr L, Schubert I, Sigle W, Trautmann C, Toimil-Molares ME. Surface enrichment in Au-Ag alloy nanowires and investigation of the dealloying process. Journal of Physical Chemistry C. 2015;**119**:20949-20956

[32] Schubert I, Sigle W, Burr L, van Aken PA, Trautmann C, Toimil-Molares ME. Fabrication and plasmonic characterization of Au nanowires with controlled surface morphology. Advanced Materials Letters. 2015;**6**:377-382. DOI: 10.5185/amlett.2015.572

[33] Schubert I, Burr L, Trautmann C, Toimil-Molares ME. Growth and morphological analysis of segmented AuAg alloy nanowires created by pulsed electrodeposition in iontrack etched membranes. Beilstein Journal of Nanotechnology. 2015;**6**:1272-1280. DOI:10.3762/bjnano.6.131

[34] Alber I, Sigle W, Demming-Janssen F, Neumann R, Trautmann C, van Aken PA, Toimil-Molares ME. Multipole surface plasmon resonances in conductively coupled metal nanowire dimers. ACS Nano. 2012;**6**:9711-9717. DOI: 10.1021/nn303149p

[35] Schubert I, Sigle W, van Aken PA, Trautmann C, Toimil-Molares ME. STEM-EELS analysis of multipole surface plasmon modes in symmetry-broken AuAg nanowire dimers. Nanoscale. 2015;**7**:4935. DOI: 10.1039/C4NR06578F

[36] Schaffer B, Hohenester U, Trügler A. High-resolution surface plasmon imaging of gold nanoparticles by energy-filtered transmission electron microscopy. Physical Review B. 2009;**79**:041401. DOI: 10.1103/PhysRevB.79.041401

[37] Bosman M, Keast VJ, Watanabe M, Maaroof AI, Cortie MB. Mapping surface plasmons at the nanometre scale with an electron beam. Nanotechnology. 2007;**18**:165505. DOI: 10.1088/0957-4484/18/16/165505

[38] N'Gom M, Li S, Schatz G, Erni R, Agarwal A, Kotov A, Norris TB. Electron-beam mapping of plasmon resonances in electromagnetically interacting gold nanorods. Physical Review B. 2009;**80**:113411. DOI: 10.1103/PhysRevB.80.113411

[39] Guiton BS, Iberi V, Li S, Leonard DN, Parish CM, Kotula PG, Varela M, Schatz GC, Pennycook SJ, Camden JP. Correlated optical measurements and plasmon mapping of silver nanorods. Nano Letters. 2011;**11**:3482-3488. DOI: 10.1021/nl202027h

[40] Nicoletti O, Wubs M, Mortensen NA, Sigle W, van Aken PA, Midgley PA. Surface plasmon modes of a single silver nanorod: An electron energy loss study. Optics Express. 2011;**19**:15371-15379

[41] Martin J, Kociak M, Mahfoud Z, Proust J, Gerard D, Plain J. High-resolution imaging and spectroscopy of multipolar plasmonic resonances in aluminum nanoantennas. Nano Letters. 2014;**14**:5517-5523. DOI: 10.1021/nl501850m

[42] Karim S, Toimil-Molares ME, Maurer F, Miehe G, Ensinger W, Liu J, Cornelius TW, Neumann R. Synthesis of gold nanowires with controlled crystallographic characteristics. Applied Physics A: Materials Science & Processing. 2006;**84**:403-407. DOI: 10.1007/s00339-006-3645-6

[43] Liu J, Duan JL, Toimil-Molares ME, Karim S, Cornelius TW, Dobrev D, Yao HJ, Sun JM, Hou MD, Mo D, Wang ZG, Neumann R. Electrochemical fabrication of singlecrystalline and polycrystalline Au nanowires: The influence of deposition parameters. Nanotechnology. 2006;**17**:1922-1926. DOI: 10.1088/0957-4484/17/8/020

[44] Dobrev D, Vetter J, Angert N, Neumann R. Periodic reverse current electrodeposition of gold in an ultrasonic field using ion-track membranes as templates: Growth of gold single-crystals. Electrochimica Acta. 2000;**45**:3117-3125. DOI: 10.1016/S0013-4686(00)00478-3

[45] Lee HO, Kim EM, Yu H, Jung JS, Chae WS. Advanced porous gold nanofibers for highly efficient and stable molecular sensing platforms. Nanotechnology. 2009;**20**:325604. DOI: stacks.iop.org/Nano/20/325604

[46] Zhang Q, Large N, Nordlander P, Wang H. Porous Au nanoparticles with tunable plasmon resonances and intense field enhancements for single-particle SERS. Nano Letters. 2014;**5**:370-374. DOI: 10.1021/jz402795x

[47] Ji C, Searson PC. Synthesis and characterization of nanoporous gold nanowires. The Journal of Physical Chemistry. B. 2003;**107**:4494-4499. DOI: 10.1021/jp0222200

[48] Ji C, Searson PC. Fabrication of nanoporous gold nanowires. Applied Physics Letters. 2002;**81**: 4437-4439. DOI: 10.1063/1.1526920

[49] Liu Z, Searson PC, Single PC. Single nanoporous gold nanowire sensors. The Journal of Physical Chemistry. B. 2006;**110**:4318-4322. DOI: 10.1021/jp056940t

[50] Ji C, Oskam G, Ding Y, Erlebacher JD, Wagner AJ, Searson PC. Deposition of Au_xAg_{1-x}/Au_yAg_{1-y} multilayers and multisegment nanowires. Journal of the Electrochemical Society. 2003;**150**:C523. DOI: 10.1149/1.1585053

[51] Johnson LP, Matisons JG. Synthesis of high aspect ratio gold nanowires with highly porous morphology. ISRN Nanomater. 2012;**2012**:1-9. DOI: 10.5402/2012/502960

[52] Yoo SH, Park S. Platinum-coated, nanoporous gold nanorod arrays: Synthesis and characterization. Advanced Materials. 2007;**19**:1612-1615. DOI: 10.1002/adma.200602551

[53] Schubert I, Huck C, Kröber P, Neubrech F, Pucci A, Toimil-Molares ME, Trautmann C, Vogt J. Porous gold nanowires: Plasmonic response and surface-enhanced infrared absorption. Advanced Optical Materials. 2016;**4**:1838-1845. DOI: 10.1002/adom.201600430

[54] Bok HM, Shuford KL, Kim S, Kim SK, Park S. Multiple surface plasmon modes for a colloidal solution of nanoporous gold nanorods and their comparison to smooth gold nanorods. Nano Letters. 2008;**8**:2265-2270. DOI: 10.1021/nl800924r

[55] Brueggeman DAG. Berechnung verschiedener physikalischer Konstanten von heterogenen Substanzen. I. Dielektrizitätskonstanten und Leitfähigkeiten der Mischkörper aus isotropen Substanzen. Annalen der Physik. 1935;**5**:656-679. DOI: 10.1002/andp.19354160802

[56] Prodan E, Radloff C, Halas NJ, Nordlander P. A hybridization model for the plasmon response of complex nanostructures. Science. 2003;**302**:419. DOI: 10.1126/science.1089171

[57] Schnell M, Garcia-Etxarri A, Huber AJ, Crozier K, Aizpurua J, Hillenbrand R. Controlling the near-field oscillations of loaded plasmonic nanoantennas. Nature Photonics. 2009;**3**: 287-291. DOI: 10.1038/nphoton.2009.46

[58] Zuloaga J, Prodan E, Nordlander N. Quantum description of the plasmon resonances of a nanoparticle dimer. Nano Letters. 2009;**9**:887-891. DOI: 10.1021/nl803811g

[59] Piraux L, George JM, Despres JM, Leroy C, Ferain E, Legras R, Ounadjela K, Fert A. Giant magnetoresistance in magnetic multilayered nanowires. Applied Physics Letters. 1994;**65**:2484-2486. DOI: 10.1063/1.112672

[60] Liu K, Nagodawithana K, Searson PC, Chien CL. Perpendicular giant magnetoresistance of multilayered Co/Cu nanowires. Physical Review B. 1995;**51**:7381-7384. DOI: 10.1103/PhysRevB.51.7381

[61] Hernández RM, Richter L, Semancik S, Stranick S, Mallouk TE. Template fabrication of protein-functionalized gold−polypyrrole−gold segmented nanowires. Chemistry of Materials. 2004;**16**:3431-3438. DOI: 10.1021/cm0496265

[62] Valizadeh S, Hultman L, George GM, Leisner P. Template synthesis of Au/Co multilayered nanowires by electrochemical deposition. Advanced Functional Materials. 2002;**12**:766-772. DOI: 10.1002/adfm.200290005

[63] Wang AA, Lee J, Jenikova G, Mulchandani A, Myung NV. Controlled assembly of multisegment nanowires by histidine-tagged peptides. Nanotechnology. 2006;**17**:3375. DOI:10.1088/0957-4484/17/14/006

[64] Nicewarner-Pena SR, Carado AJ, Shale KE, Keating CD. Barcoded metal nanowires: Optical reflectivity and patterned fluorescence. The Journal of Physical Chemistry. B. 2003;**107**:7360-7367. DOI: 10.1021/jp034139i

[65] Burdick J, Alonas E, Huang HC, Rege K, Wang J. High-throughput templated multisegment synthesis of gold nanowires and nanorods. Nanotechnology. 2009;**20**:065306. DOI: 10.1088/0957-4484/20/6/065306

[66] Cho JU, Wu JH, Min JH, Lee JH, Liu HL, Kim YK. Effect of field deposition and pore size on Co/Cu barcode nanowires by electrodeposition. Journal of Magnetism and Magnetic Materials. 2007;**310**:2420-2422. DOI: 10.1016/j.jmmm.2006.10.809

[67] Qin L, Park S, Huang L, Mirkin CA. On-wire lithography. Science. 2005;**309**:113-115. DOI: 10.1126/science.1112666

[68] Bosman M, Ye E, Tan SF, Nijhuis CE, Yang JKW, Marty R, Mlayah A, Arbouet A, Girard C, Han MY. Surface Plasmon damping quantified with an Electron Nanoprobe. Scientific Reports. 2013;**3**:1312. DOI: 10.1038/srep01312

[69] Khoury CG, Norton SJ, Vo-Dinh T. Plasmonics of 3-D nanoshell dimers using multipole expansion and finite element method. ACS Nano. 2009;**3**:2776-2788. DOI: 10.1021/nn900664j

[70] Atay T, Song JH, Numikko AV. Strongly interacting plasmon nanoparticle pairs: From dipole-dipole interaction to conductively coupled regime. Nano Letters. 2004;**4**:1627-1631. DOI: 10.1021/nl049215n

[71] Romero I, Aizpurua J, Bryant GW, Garcia de Abajo FJ. Plasmons in nearly touching metallic nanoparticles: Singular response in the limit of touching dimers. Optics Express. 2006;**14**:9988-9999. DOI: 10.1364/OE.14.009988

[72] Lassiter JB, Aizpurua J, Hernandez JI, Brandl DW, Romero I, Lal S, Hafner JH, Nordlander P, Halas NJ. Close encounters between two nanoshells. Nano Letters. 2008;**8**:1212-1218. DOI: 10.1021/nl080271o

[73] Chau YF, Lin YJ, Tsai DP. Enhanced surface plasmon resonance based on the silver nanoshells connected by the nanobars. Optics Express. 2010;**18**:3510-3518. DOI: 10.1364/OE.18.003510

[74] Perez-Gonzalez O, Zabala N, Aizpurua J. Optical characterization of charge transfer and bonding dimer plasmons in linked interparticle. New Journal of Physics. 2011. DOI:13:083013. DOI: 10.1088/1367-2630/13/8/083013

[75] Bachelier G, Russier-Antoine I, Benichou I, Jonin C, Del Fatti N, Vallée F, Brevet BF. Fano profiles induced by near-field coupling in heterogeneous dimers of gold and silver nanoparticles. Physical Review Letters. 2008;**101**:197401. DOI: 10.1103/Phys RevLett.101.197401

[76] Tumkur T, Yang X, Zhang C, Yang J, Naik GV, Nordlander P, Halas NJ. Wavelength-dependent optical force imaging of bimetallic Al-Au heterodimers. Nano Letters. 2018;**18**:2040-2046. DOI: 10.1021/acs.nanolett.8b00020

[77] Sheikholeslami S, Jun YW, Jain PK, Alivisatos AP. Coupling of optical resonances in a compositionally asymmetric plasmonic nanoparticle dimer. Nano Letters. 2010;**10**:2655-2660. DOI: 10.1021/nl101380f

[78] Flauraud V, Bernasconi GD, Butet J, Alexander DTL, Martin OJF, Brugger J. Mode coupling in plasmonic heterodimers probed with electron energy loss spectroscopy. ACS Nano. 2017;**11**:3485-3495. DOI: 10.1021/acsnano.6b08589

[79] Abb M, Wang Y, Albella P, de Groot CH, Aizpurua J, Muskens OL. Interference, coupling, and nonlinear control of high-order modes in single asymmetric nanoantennas. ACS Nano. 2012;**6**:6462-6470. DOI: 10.1021/nn3021579

[80] Shao L, Fang X, Chen H, Man YC, Wang J, Lin HQ. Distinct plasmonic manifestation on gold nanorods induced by the spatial perturbation of small gold nanospheres. Nano Letters. 2012;**12**:1424-1430. DOI: 10.1021/nl2041063

[81] Bigelow NW, Vaschillo A, Camden JP, Masiello DJ. Signatures of Fano interferences in the electron energy loss spectroscopy and cathodoluminescence of symmetry-broken nanorod dimers. ACS Nano. 2013;**7**:4511-4519. DOI: 10.1021/nn401161n@proofing

[82] Abdulla HM, Thomas R, Swathi RS. Overwhelming analogies between plasmon hybridization theory and molecular orbital theory revealed: The story of plasmonic heterodimers. Journal of Physical Chemistry C. 2018;**122**:7382-7388. DOI: 10.1021/acs.jpcc.8b00503